Resolution and Efficiency of Monitored Drift-Tube Chambers with Final Read-out Electronics at High Background Rates

J. Dubbert [b], S. Horvat [a], O. Kortner [a], H. Kroha [a], A. Manz [a], S. Mohrdieck-Möck [a], F. Rauscher [b], R. Richter [a], A. Staude [b] and W. Stiller [a]

[a] *Max-Planck-Institut für Physik*
Föhringer Ring 6
D-80805 München, Germany

[b] *Ludwig-Maximilians-Universität München*
Am Coulombwall 1
D-85748 Garching, Germany

ATL-MUON-2004-002
04 March 2004

Abstract

The performance of a monitored drift-tube chamber for ATLAS with the final read-out electronics was tested at the Gamma Irradiation facility at CERN under varyin photon irradiation rates of up to 990 Hz cm^{-2} which corresponds to 10 times the highest background rate expected in ATLAS. The signal pulse-height measurement of the final read-out electronics was used to perform time-slewing corrections. The corrections improve the average single-tube resolution from 106 μm to 89 μm at the nominal discriminator threshold of 44 mV without irradiation, and from 114 μm to 89 μm at the maximum nominal irradiation rate in ATLAS of 100 Hz cm^{-2}. The reduction of the threshold from 44 mV to 34 mV and the time-slewing corrections lead to an average single-tube resolution of 82 μm without photon background and of 89 μm at 100 Hz cm^{-2}. The measured muon detection efficiency agrees with the expectation for the final read-out electronics.

[1] Permanent address: Institut Ruđer Bošković, 10 001 Zagreb, Croatia.

1 Introduction

A BOS monitored drift-tube chamber for ATLAS which was equipped with the final front-end electronics [1] was operated in the Gamma Irradiation Facility [2] at CERN for performance studies in a high-rate environement with γ irradiation rates of up to 900 Hz cm^{-2}. Background rates between 8 Hz cm^{-2} and 100 Hz cm^{-2} are expected in the ATLAS muon spectrometer with the maximum behind the endcap toroid (see Figure 1 [3]. These estimated nominal background rates are subject to large uncertainties and could go up to 5 times the nominal rates in certain areas of the detector.

The performance studies presented here focus on the spatial resolution and the efficiency of the drift tubes. The resolution results obtained are compared with the results of previous studies [3][4]. In particular, the effect of time-slewing corrections possible with the pulse-height measurements of the the final read-out electronics is investigated.

2 Experimental Set-up

The experimental set-up which was installed in the Gamma Irradiation Facility at CERN and which is used for the test of the drift tubes with the final front-end electronics is sketched in Figure 2. The Gamma Irradiation Facility provides a 740 GBq ^{137}Cs γ source for the simulation of the ATLAS radiation background and a 100 GeV muon beam. In the set-up, a BOS monitored

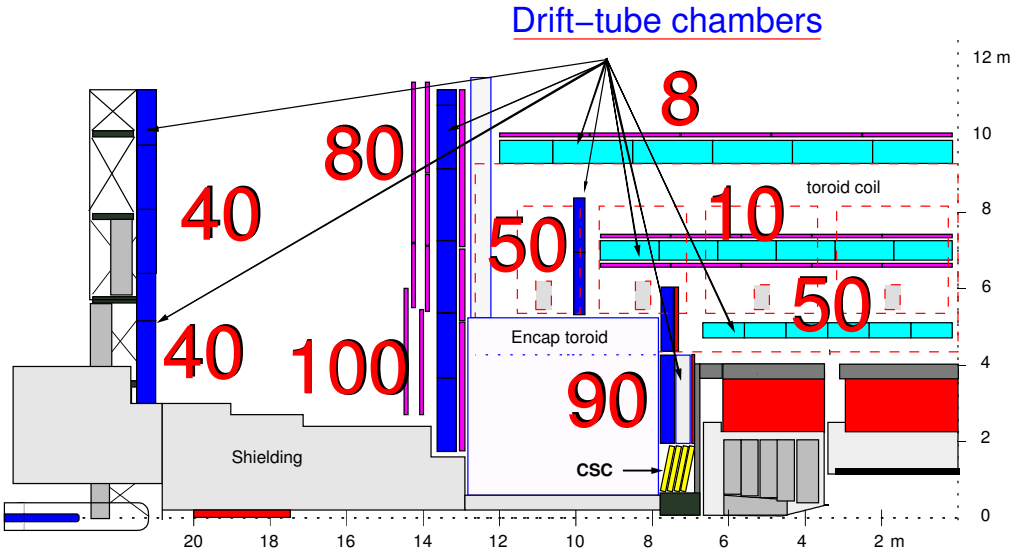

Fig. 1. Background count rates in the monitored drift-tube chambers in counts s^{-1} cm^{-2}.

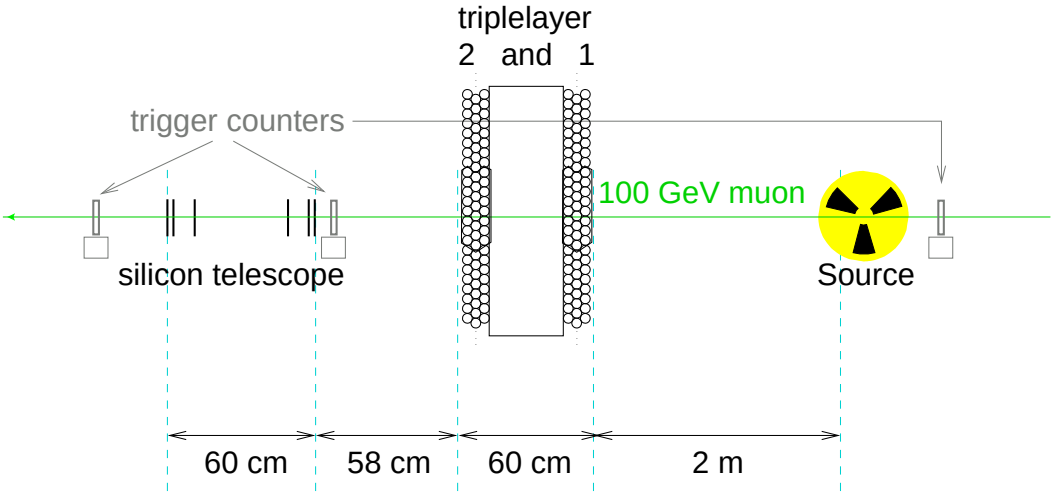

Fig. 2. Sketch of the experimental set-up (top view).

drift-tube chamber with 432 tubes of 3.8 m length and 30 mm diameter in two triplelayers is placed at 2 mm distance from the radioactive source so that count rates of up to 500 kHz per tube are reached. A telescope consisting of six layers of silicon strip detectors serves as a beam tracker. It is mounted behind the chamber in order to avoid material absorbing photons between the source and the chamber. The outer two of the silicon detectors measure the vertical beam position and the inner four the horizontal one. The telescope permits the reconstruction of the straight muon trajectories with high precision. Extrapolating a muon trajectory from the telescope into the second triplelayer (see Figure 2 for the numbering of the triple layers) gives the impact radii of the tracks in the tubes with an accuracy better than 20 μm. The sensitive areas of the silicon detectors are 5×5 cm^2.

A coincidence of the signals in four scintillation counters defines the trigger. Two crossed scintillation counters with a sensitive area of 10×10 cm^2 are installed at the entrance of the experimental zone where they are protected against the photons of the radioactive source. The other two counters with a cross section of 5×5 cm^2 enclose the beam telescope. Due to their high time resolution of better than 200 ps do they define the trigger time.

3 Data Samples

The data presented here were taken at irradiation rates ranging from 0 to about 10 times the maximum irradiation expected in the muon spectrometer. Two different threshold settings of the read-out electronics were used: the nominal setting of 44 mV and the reduced threshold of 34 mV. The dead time was always set to 790 ns, the ADC gate width to 15.5 ns. 100,000 events were taken for each setting. The characteristics of the data sets are summarized

in Table 1. The lower threshold leads to a higher sensitivity to small signals, hence to an increased photon count rate. The corrected rate in the table is the count rate which would be observed if the dead time of the electronics were 0.

Table 1
Data sets used in the analysis. 100,000 events were collected for each experimental condition.

Threshold	Measured photon count rate[1]		Corrected rate
	(kHz per tube)	($s^{-}1\,cm^{-2}$)	(kHz per tube)
44 mV	0	0	0
34 mV	0	0	0
44 mV	77±3	170±8	77±3
34 mV	84±3	187±8	84±3
44 mV	131±5	291±13	135±5
34 mV	153±6	342±13	154±6
44 mV	273±11	605±25	279±11
34 mV	302±12	670±28	311±12
44 mV	400±16	888±35	420±17
34 mV	446±18	990±40	474±19

[1]The ratio of the rate in counts per tube and in counts per cm^2 dose not corresponds to an effective tube length of 1.5 m illuminated by the radioactive source.

4 Data Analysis

The analysis of the data essentially proceeds of two steps:

(1) the reconstruction of the muon trajectories using the silicon telescope (see Section 4.1);
(2) the comparison of the *track impact radii* r_{true} in the chamber, predicted by the silicon telescope, with the *drift radii* $r(t)$, measured in the drift tubes.

Figure 3 shows the drift times measured in a tube in the second triplelayer as a function of the predicted track impact position in this tube. The distribution consists of a highly populated v-shaped band which sits on a nearly uniform background below the band. The maxima of the v-shaped band define the *space-to-drift-time* or *r-t relationship*. The width of the band is a measure of the spatial resolution. The uniform background is known to originate from δ electrons [5]. The δ electrons are knocked out of the tube walls by the incident muons and pass the sense wire at a closer distance than the muons causing a signal before the muon signal. The muon signal is not detected due to the dead time of the electronics. Hits outside the v-shaped band are rejected and contribute to the inefficiency.

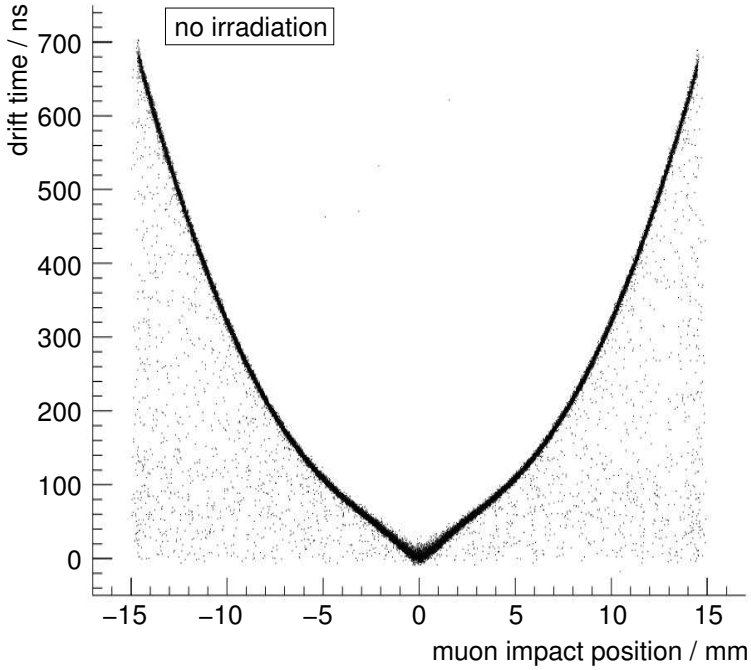

Fig. 3. Measured drift times as a function of the predicted muon impact positions in a tube of the second triplelayer without γ irradiation.

4.1 Track Reconstruction in the Silicon Telescope

The muon trajectories are reconstructed from the hits in the silicon telescope. The reconstruction is performed as described in [6]: straight lines are fitted to the positions of the hit clusters in the detector planes. Straight muon trajectories can be reconstructed in about 40% of the recorded events. The confidence-level distribution for the reconstructed trajectories is shown in Figure 4. Trajectories with confidence levels less than 0.005 are rejected. The accepted trajectories have normally distributed track-point residuals in the silicon detector planes. The standard deviations of the residual distributions

are consistent with a spatial resolution of $\leq$10 μm in the detector planes. The high spatial resolution in the detector planes guarantees that the extrapolation of the muon trajectory into the second triplelayer at a distance of 58 cm from the end of the silicon telescope has an accuracy of better than 20 μm.

4.2 Drift-Tube Resolution

4.2.1 Resolution without Corrections

The spatial resolution of the drift tubes is deteremined in two steps. in the first step, the space-to-drift-time relationship $r(t)$ is calculated by associating the impact radii r_{true} of the muon trajectories, determined with the silicon telescope, with the measured drift times t. In the second step are the deviations $\Delta r := r(t) - r_{true}$ determined as a function of r_{true} in 1 mm intervals of r_{true}.

As an example, the Δr distribution for the range 5 mm$< r_{true} <$6 mm is given in Figure 5. The distribution is normal (Gaussian) with a tail to negative values caused by δ electrons. The standard deviation of the Gaussian distribution fitted to the Δr distribution is taken as the spatial resolution of the drift tube at r_{true}=5.5 mm. The same is done in the other r_{true} intervals.

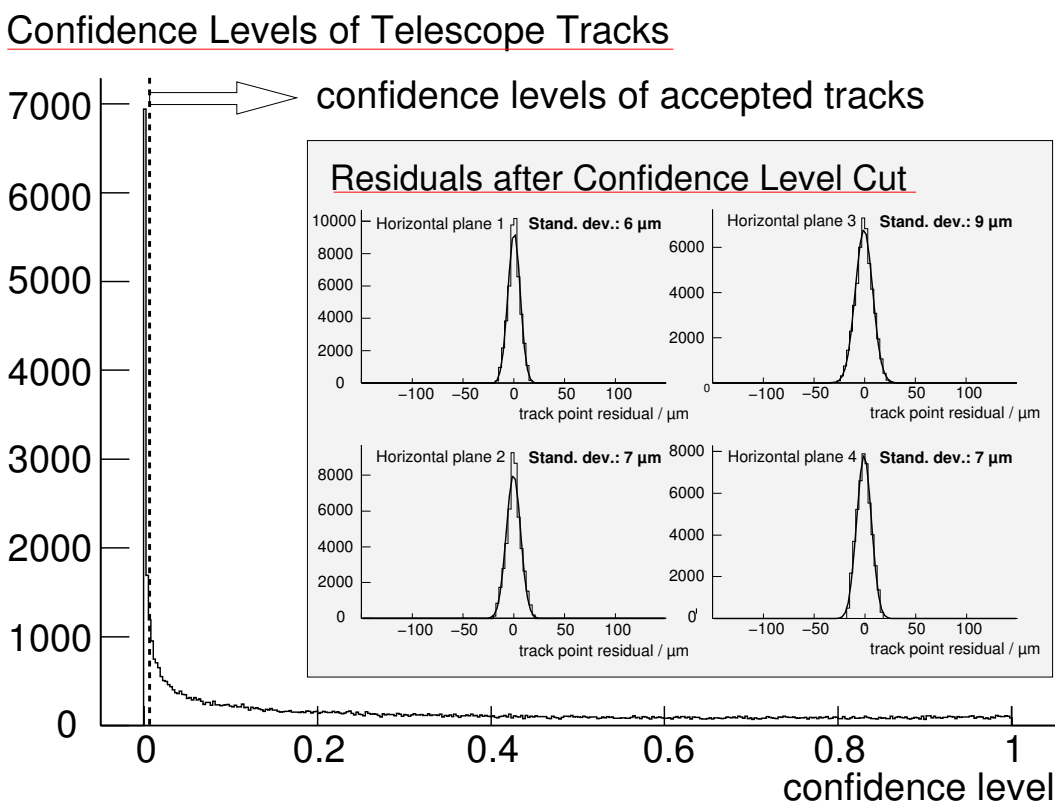

Fig. 4. Confidence level distribution and track point residuals for accepted tracks reconstructed in the silicon telescope.

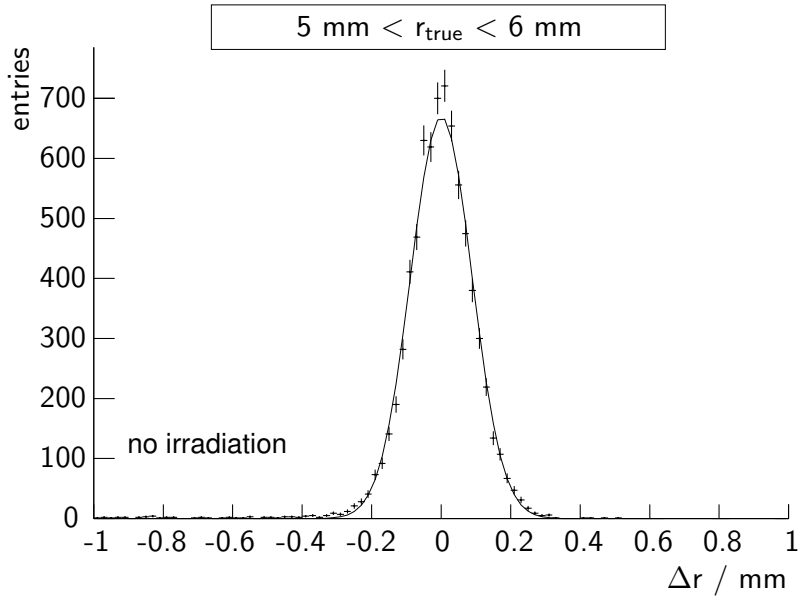

Fig. 5. Deviation Δr of the measured drift radii $r(t)$ from the muon impact radii r_{true}.

This procedure is not perfectly adequate for muon hits in the vicinity of the anode wire of a tube. This is illustrated in Figure 6 for 0< r_{true} <1 mm. The Δr distribution is asymmetric towards positive Δr values in this region. The asymmetry originates from the fact that the distances of the primary ionization clusters along the muon trajectory show large fluctuations up to values much larger than r_{true} itself. This is visualized in Figure 7. A Gaussian fit to the

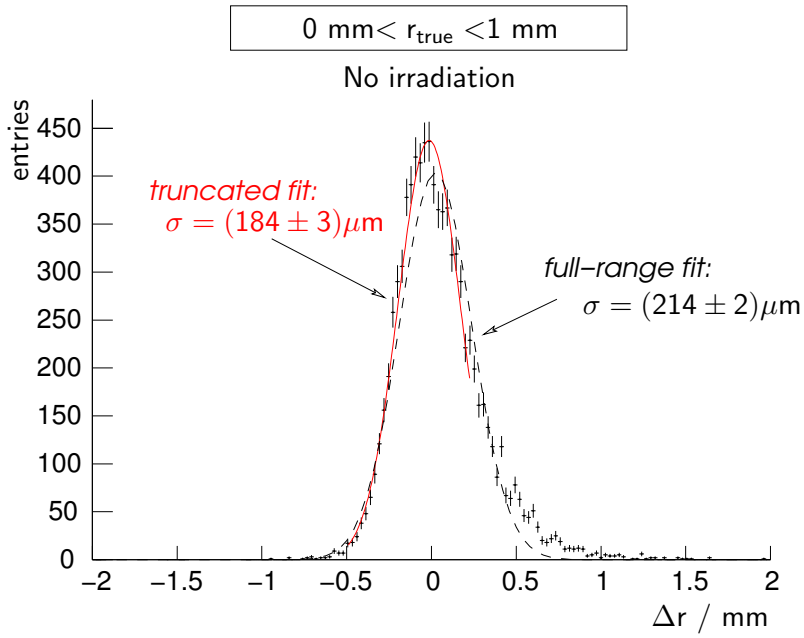

Fig. 6. Deviations Δr of the measured drift radii $r(t)$ from the muon impact radii r_{true} in the vicinity of the anode wire of a tube.

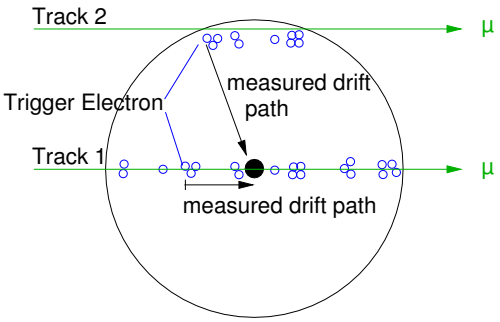

Fig. 7. Illustration of the distribution of primary ionization clusters for muon trajectories far away and close to the sense wire..

asymmetric distribution is used in the present analysis for the estimation of drift-tube resolution at small radii, too. This results in large, but more conservative estimates of the spatial resolution at small radii than a truncated fit which better resembles the peak region of the Δr distributions would yield. A better estimate would be the width of that interval around the peak of the asymmetric distribution which contains 66% of the distribution. The spatial resolution as a function of r_{true} is shown in Figures 8 and 9 for both threshold settings (44 mV and 34 mV respectively) and different γ irradiation rates. If the drift-tube chamber is not irradiated, the resolution is about 230 μm for hits close to the wire improving to about 60 μm at large impact radii. The resolution is degraded with increasing γ background rate. The γ particles from the radioactive source are converted into electrons which ionize the gas in the drift tubes. The space charge from the ionization alters the electric field inside

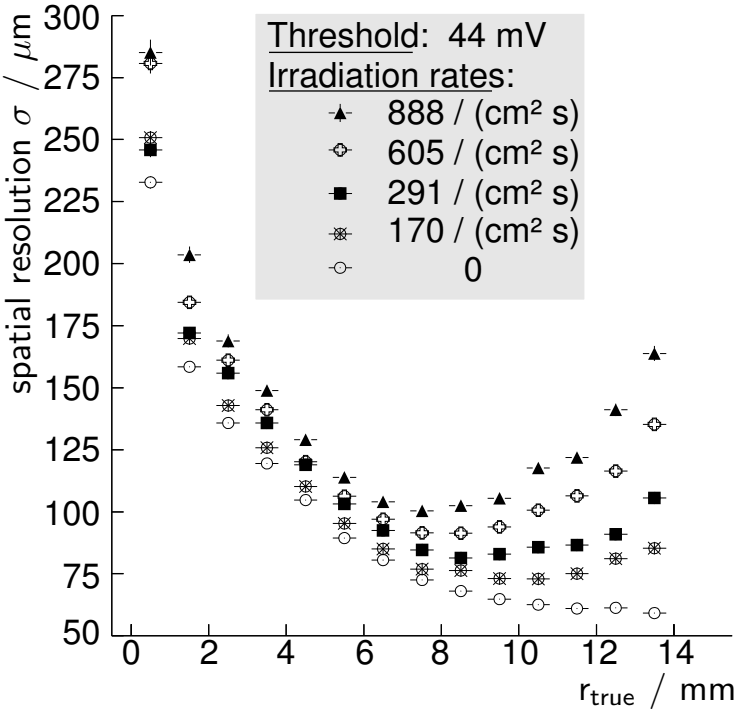

Fig. 8. Spatial resolution curves obtained with the nominal threshold of 44 mV.

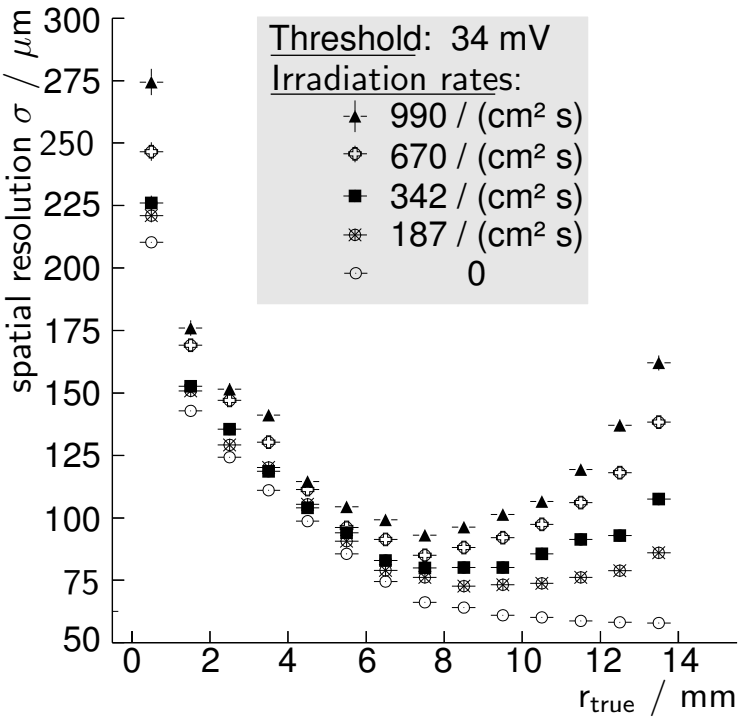

Fig. 9. Spatial resolution curves obtained with the reduced threshold of 34 mV..

the drift tube. Since the drift velocity depends on the electric field in case of the $Ar/CO_2(93/7)$ gas mixture, the r-t relationship is affected bythe space charge created by the background irradiation. Fluctuations in the ionization and the space charge of the background irradiation cause fluctuations of the r-t relationship which deteriorate the spatial resolution. The fluctuations increase with increasing irradiation rate. As the effect sums up along the drift path, the resolution degradation increase with increasing radius (see Figures 8 and 9).

Since the drift distance ideally tends to zero when the impact radius goes to zero, one would expect no resolution degradation in the limit $r_{true} \rightarrow 0$. But this is not observed. A degradation of up to 50 μm is measured. For hits in the vicinity of the anode wire, the drift distances of the electrons from primary clusters vary strongly as mentioned earlier. Therefore, the arrival times of those electrons which have to travel a long distance are affected by the space-charge fluctuations. The tail of the asymmetric Δr distribution becomes larger, as shown in Figure 10. The full-range fit is sensitive to this so that a degraded resolution is measured. It is interesting to mention that the width of the truncated fit is almost insensitive to this effect. Another origin of a resolution degradation at small radii is the gain drop which increases with increasing irradiation. A simulation of the space-charge and the gain-drop effect within a Garfield [7] calculation is needed to quantify the contribution of both effects to the resolution degradation at small radii. We postpone this study to another note.

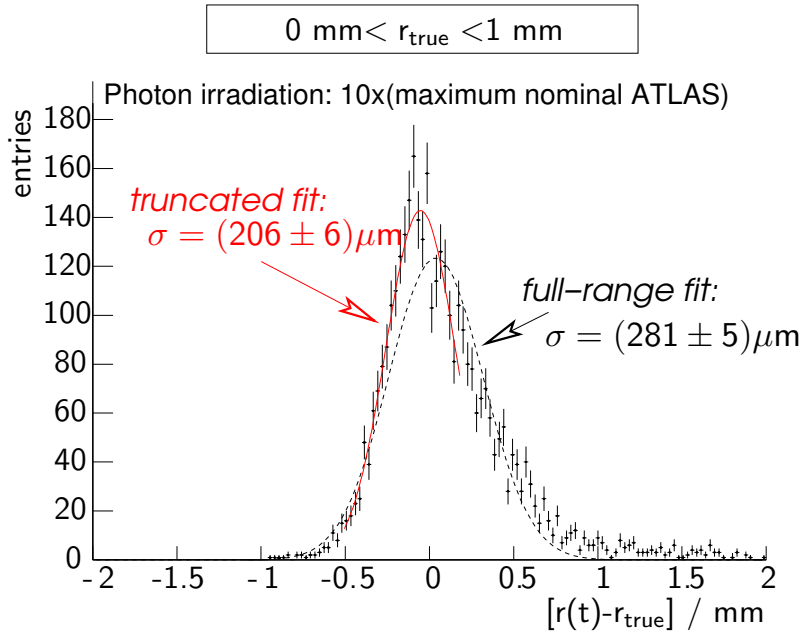

Fig. 10. Deviations Δr of the measured drift radii $r(t)$ from the muon impact radii r_{true} in the vicinity of the anode wire of a tube.

4.2.2 Threshold Dependence and Choice of the Lower Threshold

Figure 11 shows the improvement of the spatial resolution which is obtained with the lower discriminator threshold. Reducing the threshold from 44 mV to 34 mV leads to an average resolution improvement of 17 μm for impact radii between 0 and 5 mm. There is little improvement at larger radii. The spatial resolution $\sigma(r)$ is connected with the drift uncertainty δt by the equation $v(t) \cdot \delta t = \sigma(r)$. The drift velocity in $Ar/CO_2(93/7)$ is about 0.05 mm ns^{-1} for $0 \leq r \leq 5$ mm and about 0.017 mm ns^{-1} for $r > 5$ mm. Therefore, one can conclude that δt improves by 17 μm/0.05 mm ns^{-1}=0.34 ns at small radii. An improvement in the time-measurement uncertainty of the order of 0.344 ns should lead to a resolution improvement of about 0.34 ns·0.017 mm ns^{-1}=6 μm

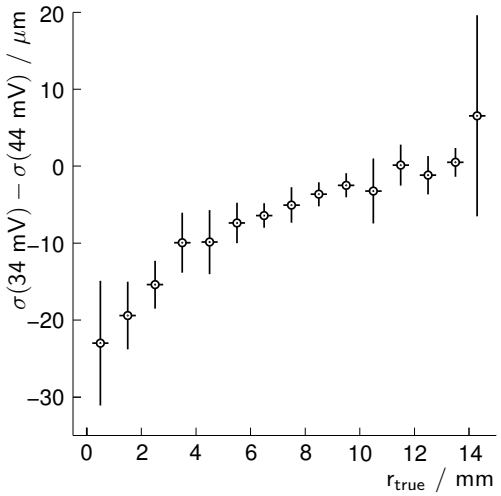

Fig. 11. .Resolution improvement with the lower threshold (34 mV instead of 44 mV). The improvement shown here is an average of the improvements obtained at the different irradiation rates. This average is justified because the improvements are very similar.

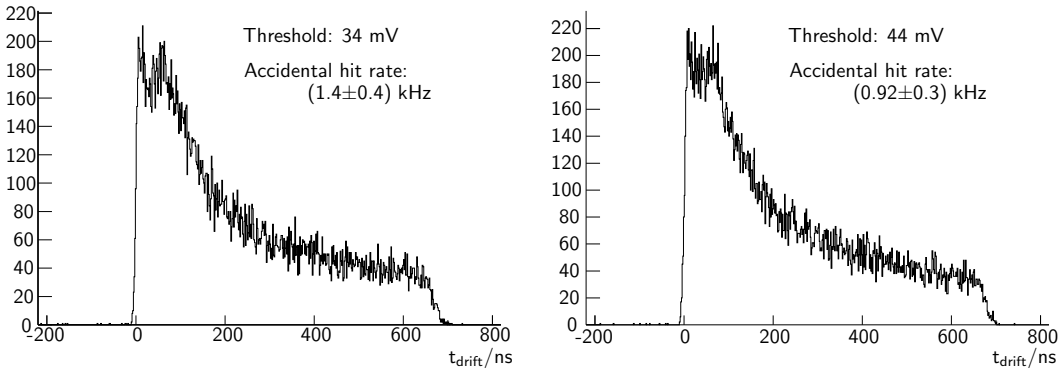

Fig. 12. Drift-time spectra obtained with the 34 mV and 44 mV threshold in a uniformely illuminated tube of the chamber.

at large r which is in agreement with the observed improvement.

Lowering the treshold from 44 mV to 34 mV leads to an increase of the accidental hit rate by a factor 1.5 only, as demonstrated in Figure 12 where the drift-time spectra in a uniformely illuminated tube obtained with both thresholds are shown. The accidental hit rate is small ($\approx$1 kHz) in both cases. So lowering the threshold from 44 mV to 34 mV can be considered. A further significant reduction of the threshold cannot be recommended because the accidental hit rate grows exponentially when the treshold is set to values below 30 mV.

4.3 Time-Slewing Corrections

Signals with large pulse heights cross the discriminator threshold earlier than signals with small pulse heights. As a consequence, the measured drift times and radii become smaller with increasing pulse heights. The Wilkinson ADC

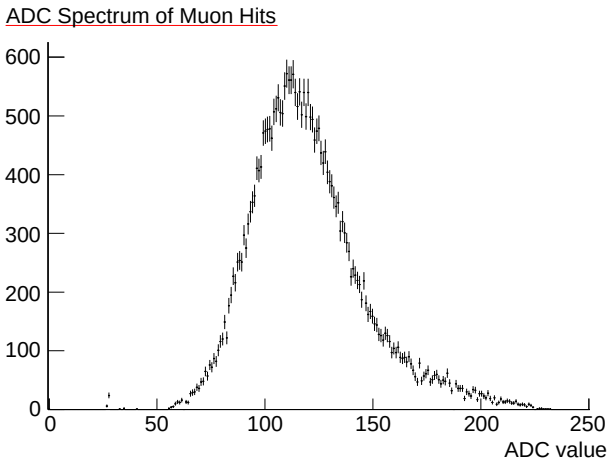

Fig. 13. Pulse-height spectrum of muon hits in a drift tube.

of the final read-out electronics measures the charge integrated in the 15.5 ns after the threshold crossing which is proportional to the pulse height [1]. The pulse-height spectrum for muon hits is presented in Figure 13. The spectrum has the expected shape of a Landau distribution.

The deviations Δr of the drift radii from the tru radii are plotted versus the inverse pulse heights of the corresponding muon signals for 13 mm< r_{true} <14 mm in Figure 14. Hits with large pulse heights, i.e. small inverse pulse heights, tend to have smaller radii than hits with small pulse heights. The dependence of Δr on the inverse pulse height can be parametrized by a parabolic function. The parametrization can be used to correct Δr for the pulse-height dependence.

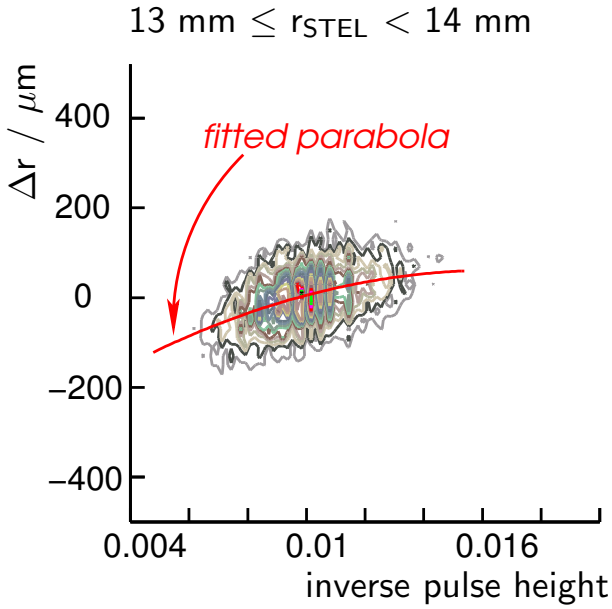

Fig. 14. Dependence of Δr on the inverse pulse height.

As shown in Figure 15, this correction leads to an average improvement of the spatial resolution of about 30 μm for radii $\leq$5 mm and of about 10 μm for radii >5 mm which is almost independent of the threshold and the background irradiation rate. The dependence of the resolution improvement on r can be explained by the variation of the drift velocity in the same way as in Section 4.2.1. The average drift velocity is about 0.05 mm ns^{-1} for $r \leq 5$ mm and about 0.017 mm ns^{-1} for $r > 5$ mm. If the time slewing is of the same order in bot r regions, the ratio of the resolution improvements in both r regions should equal the ratio 2.5 which is approximately the case.

The improvements in the average single-tube resolution defined as the quadrativ average of the resolution $\sigma(r)$ over the whole impact radius range, i.e.

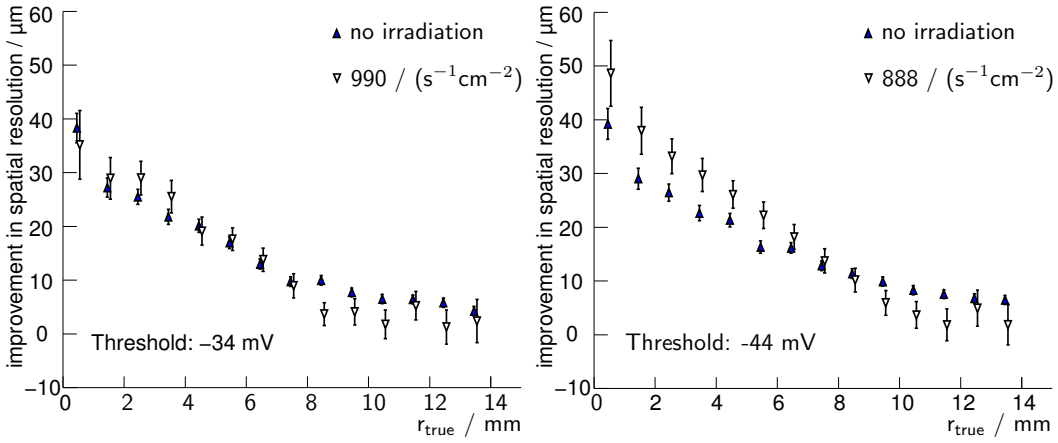

Fig. 15. Improvement of the spatial resolution using time-slewing corrections for two different discriminator thresholds and irradiation rates.

$$\sqrt{\frac{1}{r_{max}} \int_0^{r_{max}} \sigma^2(r)\, dr},$$

are illustrated in Figure 16: (a) for the nominal threshold setting (44 mV) without time-slewing corrections, (b) the nominal threshold setting with time-slewing corrections, and (c) for the reduced threshold (34 mV) with time-slewing corrections. In the first case, the resolution is always greater than 100 μm which is the minimum requirement for the design resolution of the

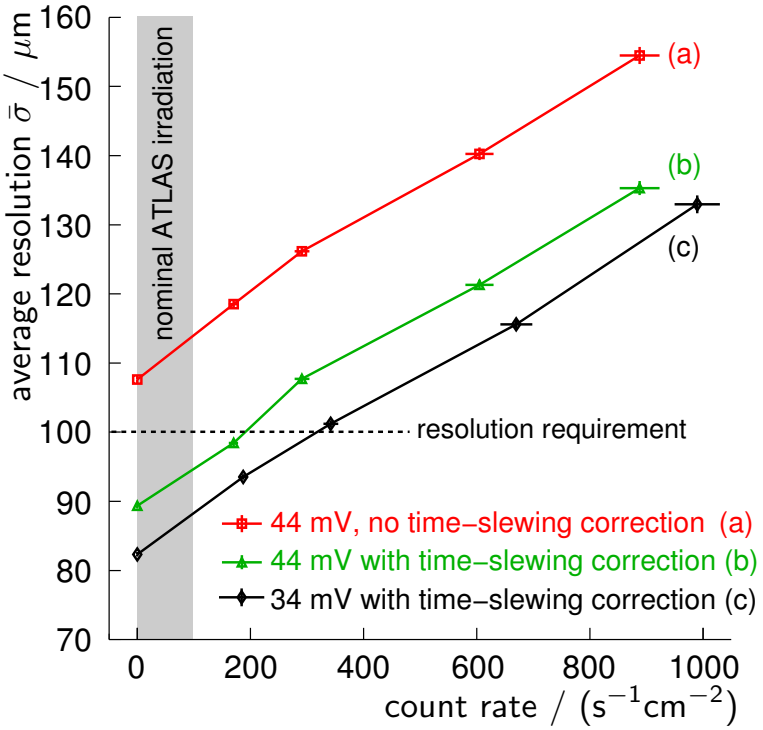

Fig. 16. Average single-tube resolution $\bar{\sigma}$ as a function of the irradiation rate for different threshold settings.

muon spectrometer. The time-slewing corrections lead to an improvement of the resolution by 18 μm independently of the irradition rate. The resolution stays below 100 μmup to twice the maximum nominal ATLAS background rate. Lowering the threshold to 34 mV in addition leads to a resolution of 32 μm without γ irradiation and of better than 100 μm up to 3 times the expected maximum irradiation rate. In this way, the resolution specifications of the Technical Design Report [8] are achieved with the non-linear Ar/CO_2 gas mixtureand the final read-out electronics with shielded hedgehog boards.

4.3.1 Comparison with Previous Measurements

In 2002 a BOS chamber equipped with unshielded read-out hedgehog cards and the prototype version of the mezzanine cards was tested in the high-rate environment of the Gamma Irradiation Facility [4]. The shielding on the hedgehog cards was shown to diminish the spatial resolution by about 5 μm at small radii due to the additional capacitance introduced which reduces the pulse heights [9]. The prototype mezzanine cards use unipolar shaping with an undershoot of the pulses while the final cards have bipolar shaping. The spatial resolution curves obtained with the final cards at their nominal threshold of 44 mV are in accord with the curves obtained with the prototype cards at their nominal threshold of 60 mV. The resolution curves with the final cards at 34 mV threshold agree with the curves obtained with the prototype cards at 46 mV threshold. In reference [4] the resolution curve obtained with the prototype cards at 46 mV threshold was found to reproduce the results obtained with the BNL electronics at a threshold corresponding to the 25th primary electron [10]. We therefore assume that the 46 mV threshold on the prototype cards and the 34 mV threshold on the final cards correspond to the 25th primary electron. Using the fact that the ratio of the spatial resolutions σ_1 and σ_2 near the wire ($r \to 0$), taken at the thresholds $U_{t,1}$ and $U_{t,2}$ respectively, equals the square root of the ratio $U_{t,1}/U_{t,2}$ [5], we can conclude that the nominal thresholds of both mezzanine card versions correspond to the 28th primary electron. Since the nominal threshold is defined as the voltage corresponding to 6 times the thermal noise at the input of the discriminator, the reduced threshold of 34 mV on the final card corresponds to 4.6 times the thermal noise.

Before the ATLAS read-out electronics became available, the drift tubes were operated in the Gamma Irradiation Facility with the BNL amplifiers connected directly to the tubes without an intermediate hedgehog card [3]. This read-out leads to a lower thermal noise and allows for a lower discriminator threshold corresponding to the 18th primary electrons which was measured to be 5 times the thermal noise. The low threshold improves the resolution for hits close to the anode wire by 30 μm compared to the final read-out electronics. The time-slewing corrections possible with the final electronics compensate for the

higher required threshold.

4.4 Efficiency Determination

We turn to the measurement of the muon detection efficiency of a single tube.

When a muon traverses a drift tube and a hit is registered by the tube, the detected hit may be caused by the muon itself, δ electrons or background ratiation. The *hit efficiency* measures the probability that a tube has at least one hit when it is traversed by the muon. It does not distinguish between muon, δ electron, and background radiation hits.

The hit efficiency is expected to decrease with increasing photon irradiation. When the read-out electronics receives a trigger signal, tube hits are recorded only if the arrival time falls inside a time window around the trigger time (see Figure 17), which we call this window the *trigger acceptance window*. In addition, no hit is recorded if the time falls into the fixed dead time window of 790 ns after a previous hit taking place at a time before the trigger acceptance window.

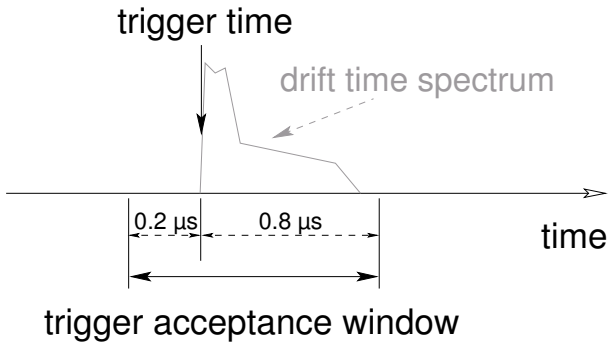

Fig. 17. The trigger acceptance window, i.e. the time window with respect to the trigger time in which tube hits are recorded.

This effect is seen in the data. The measured hit efficiency in Figure 18 decreases with increasing photon irradiation. The decrease is higher at smaller impact radii, because small radii correspond to small drift times. In the extreme case of 474 kHz per tube irradiation rate, the hit efficiency drops to 90%. Figure 18 also shows that the drift tubes are efficient for muons reconstructed in the silicon telescope if there is no background irradiation. The efficiency drop for hits close to the tube walls is a consequence of the short path of the muons inside the gas volume. If this path becomes too short, not enough primary electrons are created to cross the signal threshold.

The *3σ efficiency* measures the probability that the measured drift radius $r(t)$ agrees with r_{true} within $\pm 3\sigma(r_{true})$ where $\sigma(r_{true})$ is the spatial resolution of

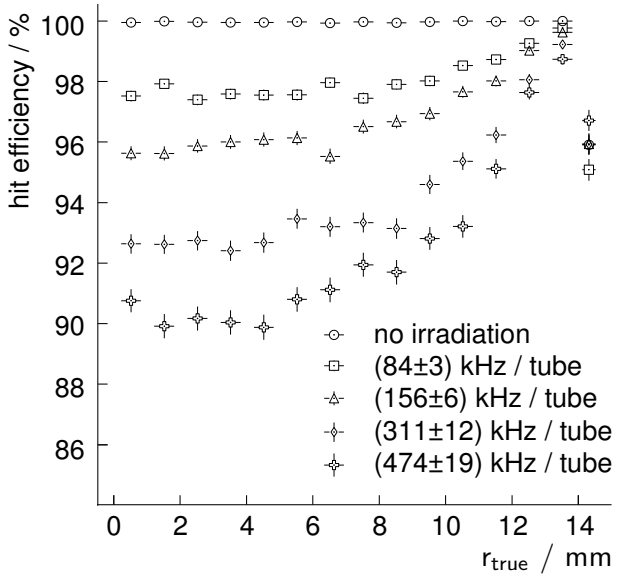

Fig. 18. Hit efficiency as a function of the impact radius r_{true} and the photon irradiation rate.

the tube at radius r_{true}.

The 3σ efficiency decreases with increasing photon irradiation rate. Photons which are detected at an earlier time than the muon cause hits with wrong drift times which translate into wrong drift radii. The measured dependence of the 3σ efficiency on the photon irradiation rate is shown in Figure 19. It is

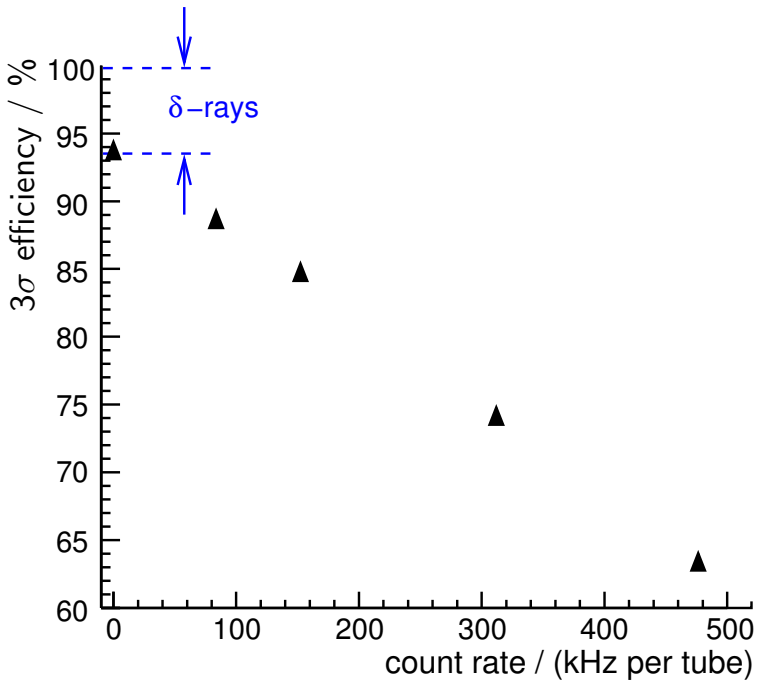

Fig. 19. Measured 3σ efficiency as a function of the background irradiation rate.

93.5% without photon background and drops to 64% at a background count rate of about 474 kHz per tube. It is below 100% without photon background because of δ electrons which are knocked out of the tube walls and pass the tube anode wires at distances smaller than the muon, hence causing hits at an earlier times than the muon would.

The prediction of the measured 3σ and the hit efficiencies is not trivial. It requires a detailed simulation of the drift-tube response to muons, photons, and δ electrons as well as the correct simulation of the δ hit production. We postpone this simulation study to a later article.

Yet the *total muon-hit efficiency* which is the product of the muon hit efficiency and the 3σ efficiency can be predicted by calculating the probability that a δ electron or background photon hit may mask a muon hit when it occurs earlier than the muon hit. In this calculation, the probability of a δ electron hit is taken from the measurement of the total efficiency without photon background. The measured total hit efficiency ande the prediction as a function of the photon irradiation rate are presented in Figure 20. The prediction is in accord with the measured efficiencies up to rates corresponding to five times the maximum nominal irradiation rate in ATLAS. The measured total efficiency is 10% below the prediction at the highest background rate of 500 kHz per tube. The disagreement of prediction and measurement at very high rates must still be understood. We expect that the discrepancy will be resolved by the detailed simulation which is under preparation.

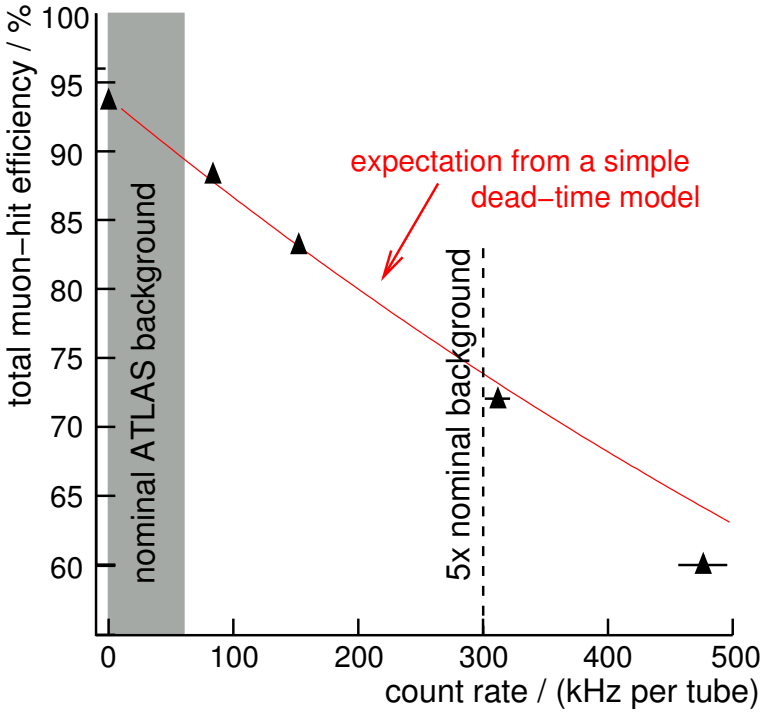

Fig. 20. Total muon-hit efficiency as a function of the background irradiation rate.

5 Summary

The performance of the final MDT front-end electronics was tested at photon irradiation count rates ranging from zero to 990 Hz cm^{-2}, which corresponds to 10 times the maximum nominal irradiation rate in ATLAS. The read-out electronics was operated at two different discriminator thresholds, the nominal threshold of 44 mV and the reduced threshold of 34 mV which is still acceptable because of a low accidental hit rate. The average spatial resolution of a drift tube is 106 μm at thee nominal treshold already without irradiation. Time-slewing corrections using the pulse-height measurement implemented in the final electronics improve the average resolution by 15 μm. As a consequence, the average spatial resolution is better than 100 μm for up to twice the maximum nominal irradiation rate in ATLAS. Operating at a reduced threshold of 34 mV and applying the time-slewing corrections, the design goal of 80 μm spatial resolution is reached with the $Ar/CO_2(93/7)$ gas mixture without photon background and an average resolution of better than 100 μm is maintained for up to 3 times the maximum nominal background rate in ATLAS.

The single-tube efficiency decreases at most linearly with increasing background irradiation. The measured hit efficiencies are quantitatively described by a simple dead-time model of the read-out electronics up to rates of 5 times the maximum nominal irradiation rate in ATLAS.

Acknowledgements

We would like to thank a few colleagues for their help: M. Deile for the fine-tuning of the silicon telescope, J. Chapman and J. Gregory for the support on the new electronics, and S. Haas for repairing an important hardware component.

References

[1] C. Posch et al., *CMOS front-end for the MDT sub-detector in the ATLAS Muon Spectrometer – development and performance*, contribution to the 7th Workshop on Electronics for LHC Experiments LEB 2001 , Stockholm, Sweden , 10 - 14 Sep 2001 - pages 199-203.

[2] S. Agosteo, *A facility for the test of large-area muon chambers at high rates*, Nuclear Instruments and Methods in Physics Research A 452 (2000) 94-104.

[3] M. Aleksa et al., *Rate effects in high-resolution drift chambers*, Nuclear Instruments and Methods in Physics Research A 446(2000) 435-443.

[4] M. Deile et al., *Resolution and Efficiency Studies with a BOS Monitored Drift-Tube Chamber and a Silicon Telescope at the Gamma Irradiation Facility*, ATLAS internal note ATL-COM-MUON-2003-006.

[5] M. Deile, *Optimization and Calibration of the Drift-Tube Chambers for the ATLAS Muon Spectrometer*, doctoral thesis, Munich 2000.

[6] M. Deile et al., *ODYSSEUS- a Silicon Telescope for Test-Beam Experiments*, ATLAS internal note ATL-COM-MUON-99-15.

[7] R. Veenhof, *GARFIELD: Simulation of gaseous detectors, Version 6.21*, CERN.

[8] The ATLAS Muon Collaboration, *ATLAS Muon Spectrometer – Technical Design Report*, CERN/LHCC 97-22, Geneva 1997.

[9] S. Horvat et al., *Study of the Resolution of Monitored Drift-Tube Chambers with Shielded Hedgehog Cards*, ATLAS internal note ATL-COM-MUON-2003-004.

[10] F. Bauer et al., *Construction and Test of MDT Chambers for the ATLAS Muon Spectrometer*, ATLAS internal note ATL-MUON-2001-006 (2000) and Nucl. Instrum. and Methods, A 461 (2001).